PAPER

Check for updates

Interface exciplex formation in TADF organic light-emitting transistors

Amirhossein Azari, [ID] *[a] Georgios Fanourakis,[a] Shujie You,[c] Isabella Concina [ID] [c] and Caterina Soldano *[ab]

Thermally-activated delayed fluorescence (TADF) materials have received significant attention for their ability to harvest both singlet and triplet excitons *via* reverse intersystem crossing (rISC), enabling near 100% internal quantum efficiency without relying on scarce heavy-metal complexes. While TADF emitters are largely used in organic light-emitting diodes (OLEDs), their implementation in organic light-emitting transistors (OLETs), a device platform that uniquely combines transistor switching and light emission, remains relatively underexplored. In this work, we fabricated and investigated the integration of 2CzPN, a blue-emitting TADF molecule, doped into the high-triplet-energy host DPEPO in different architectures to explore their potential for efficient and colour-tunable light emission. We explored multilayer heterostructures which include (or not) an electron transport layer, and we found that an approximate 10 wt% doping of 2CzPN in the DPEPO host yielded optimal performance in all cases. However, two-layer devices (no electron transport layer) exhibited intrinsic emission, typical of 2CzPN, while the addition of the electron transport layer led to both a redshift of the emission (green emission) and the onset of an additional spectral contribution due to the formation of interfacial exciplexes at the emissive layer/*e*-transport interface. Our results demonstrate the dual advantage of TADF emitters in field-effect devices: efficient triplet harvesting and tunable emission *via* interface engineering, thus suggesting the importance of optimizing both emitter design and device architecture for high-performance, color-tunable organic transistors.

1. Introduction

Organic electronic materials have gathered continuously increasing and significant attention as promising candidates for next-generation optoelectronic applications, due to their distinctive advantages such as low-cost processability, light weight and flexible form factors, and the ability to fine-tune their optical and electronic properties *via* molecular design.[1–3] These characteristics are particularly advantageous in applications like wearable and flexible electronics, where traditional inorganic and CMOS-based systems face intrinsic limitations due to material rigidity and resource scarcity.[4] Organic materials can be precisely engineered through synthesis to achieve specific functionalities, are generally inexpensive, and in some cases biocompatible; they are suitable and easy to integrate into low-cost manufacturing processes, while offering a more environmentally-friendly route for end-of-life disposal.[4]

Upon demonstration of semiconducting behaviour in organic molecules, the field of organic electronics has seen a rapid expansion;[5,6] for example, organic light-emitting diodes (OLEDs) are currently routinely commercialized for applications mainly in display and lighting technologies, due to their high electroluminescence efficiency, excellent colour quality, and compatibility with diverse substrates.[2,7] OLEDs rely on a vertical device architecture (and corresponding vertical charge transport), which requires at least one transparent electrode to extract the light, thus introducing device complexity and cost.[7]

In recent years, organic light-emitting transistors (OLETs) have emerged as a potential light-emitting (and sensing) device, alternative and/or complementary to OLEDs.[8] OLETs integrate the light-emission functionality of OLEDs with the switching behaviour of field-effect transistors within a planar, lateral structure.[9] This enables spatial modulation of emission, releases the requirement for transparent electrodes (light can be generated in the channel), and can potentially enable simplified, pixel-integrated optoelectronic components.[10,11] Although this device platform is still not fully understood and developed yet, it has been shown that it can potentially outperform OLEDs equivalent in terms of device efficiency when using the same set of materials.[12]

[a] *Department of Electronics and Nanoengineering, School of Electrical Engineering, Aalto University, 02150 Espoo, Finland. E-mail: amirhossein.azari@aalto.fi*

[b] *Department of Physics, Northeastern University, 02115 Boston, MA, USA*

[c] *Department of Engineering Sciences and Mathematics, Luleå University of Technology, 97187 Luleå, Sweden*

23028 | *J. Mater. Chem. C*, 2025, **13**, 23028–23036

This journal is © The Royal Society of Chemistry 2025

Achieving high-performance organic light-emitting transistors requires simultaneous optimization of several parameters, including organic semiconductors exhibiting high charge carrier mobility for efficient transport,[13,14] highly efficient emissive materials for bright light generation,[15] dielectric interface engineering[16] and suppression of interfacial trap states.[17,18]

State-of-the-art OLETs have achieved notable external quantum efficiencies (EQEs) up to 8% for fluorescent emitters,[19] with some devices demonstrating high brightness exceeding 1000 cd m^{-2} and good stability while using van der Waals-like heterojunctions and optical microcavities.[19–21]

In terms of emissive organic materials and their efficiency, the introduction of thermally-activated delayed fluorescence (TADF) emitters by Adachi's group in 2012 represented a key advancement.[22] TADF materials overcome the 25% internal quantum efficiency (IQE) limitation inherent to conventional fluorescent emitters by using reverse intersystem crossing (rISC) to harvest triplet excitons *via* thermal activation, thereby achieving nearly 100% IQE without the need for heavy-metal complexes.[23,24] These purely organic emitters are typically designed with donor and acceptor moieties that minimize the singlet–triplet energy gap (ΔE_{ST}), enhancing rISC and enabling efficient emission from both singlet and triplet states.[25–28] Compared to phosphorescent emitters, TADF molecules offer similar efficiencies while reducing cost and need for rare-earth elements and improving the colour stability (especially in the blue spectral region). Advancements in molecular design have further improved device performance, with the reported EQE exceeding 30–40% in OLEDs, alongside narrowband emission.[29]

Despite the growing use of TADF materials in OLEDs in the last few years, their integration into field-effect light-emitting transistor architectures has remained relatively unexplored. Early demonstrations used intermolecular TADF exciplex systems such as TCTA:B3PYMPM, which achieved modest performances, including EQEs around 1% and luminance values over 1000 cd m^{-2}.[30] Further work on intramolecular TADF emitters, including 4CzIPN and ACRXTN, has shown improvements in brightness levels (100–1000 cd m^{-2}) and carrier modulation, while values of EQE remain limited primarily due to light outcoupling efficiency and optical losses near the metallic contacts.[9] Laterally integrated OLETs exploiting optical amplification due to optical microcavities have also shown promising results in terms of efficiency and colour purity for red and green colours.[19]

In this work, we report the fabrication and optoelectronic characterization of bottom-gate, top-contacts multilayer heterostructure organic light-emitting transistors employing the TADF emitter 2CzPN. Light emission is achieved through a host–guest system, with 2CzPN doped into the wide-gap, high-triplet-energy host DPEPO, facilitating efficient exciton confinement and radiative recombination. Our results show that (a) emitter concentration of approximately 10 wt% doping ratio of 2CzPN yields improved performance in terms of light output efficiency and carrier modulation and (b) the presence of the electron transport layer (on top of the emissive layer) leads to a shift in the electroluminescence spectrum from sky-blue emission with colour coordinates (0.26, 0.50) to green emission with coordinates (0.18, 0.38) as well as an additional spectral component (at 570 nm) which we attributed to the formation of interfacial exciplexes at the boundary of such interface.

2. Experimental details

2.1. Device fabrication

Glass substrates with pre-patterned indium tin oxide (ITO) were initially cleaned according to the following protocol: sonication for 10 minutes in a diluted Hellmanex III solution, then in deionized (DI) water for 5 minutes, twice in acetone for 10 minutes each and in 2-propanol for 10 minutes. Substrates were dried using nitrogen and then treated with oxygen plasma (100 W power for 15 minutes) to promote hydrophilicity prior to the dielectric layer deposition. A solution of polymethyl methacrylate (PMMA, Allresist AR-P 679.24) was then spin-coated onto the substrates and then annealed at 110 °C for 30 minutes under ambient conditions to remove any residual solvent. Organic semiconductor materials and silver electrodes were deposited *via* thermal evaporation in a Moorfield Nanotechnology Mini-Lab90 system. The organic semiconductors, 2,7-dioctyl1benzothieno3,2-b1benzothiophene (C8-BTBT, Sigma Aldrich) and 5,5'-bis((5 perfluorohexyl)thiophen-2-yl)-2,2'-bithiophene (DFH-4T, Sigma Aldrich), were deposited at a rate of 0.1 Å s^{-1}, while the host material, bis[2-(diphenylphosphino)phenyl]ether oxide (DPEPO) and the silver were deposited at a rate of 1 Å s^{-1}. The deposition rate of the guest material, 1,2-bis(carbazol-9-yl)-4,5-dicyanobenzene (2CzPN), was adjusted relative to the host to achieve different doping concentrations within the blend. All thermal evaporation processes were conducted under a high vacuum environment at a base pressure of 10^{-7} mbar. The evaporation chamber is directly integrated with a glovebox, where samples are transferred and characterized.

2.2. Film characterization

Film thickness was measured using a Dektak XT stylus profilometer, while the surface morphology was investigated utilizing an atomic force microscope (AFM, Bruker Dimension Icon) scanning over an area of 10 μm × 10 μm. Photoluminescence was collected using a custom-built spectroscopic system, including a He-Cd laser (λ_{exc} = 325 nm) as the excitation source, and an IR2000 spectrometer to collect the emitted light. An optical density (OD) 2.0 filter was incorporated into the optical path to mitigate potential high excitation power effects. Optical absorbance spectra were recorded using a Shimadzu UV-2600 spectrophotometer, configured with a slit width resolution of 1.0 nm and an accumulation time of 2 seconds. The time-resolved photoluminescence (TRPL) spectra were recorded with an Edinburgh FLS980 spectrofluorometer equipped with a 372 nm nanoseconds pulsed diode laser (pulse width 64.0 ps), used for the short decay spectra, and an nF2 microseconds Flashlamp, used for the long decay spectra, from Edinburgh Instruments. The system was equipped with an integrating

sphere and the spectra were recorded using identical excitation and emission wavelengths.

2.3. Device optoelectronic characterization

Electro-optical characterization of the fabricated devices was performed within a glovebox with a controlled environment at room temperature. A Keysight B1500A semiconductor parameter analyzer was used for acquiring electrical data. The light output intensity was measured using a Hamamatsu S1337 photodiode positioned in direct contact with the substrate (bottom emission). Collecting top emission from the device is beyond our current experimental capabilities. Electroluminescence spectral data were collected using a Konica Minolta CS-2000 spectroradiometer.

3. Results and discussion

3.1. Photoexcitation in DPEPO:2CzPN blends

Fig. 1a shows the normalized photoluminescence (nPL) of DPEPO:2CzPN blends with different 2CzPN contents (60 nm, solid line) deposited on quartz; the corresponding photoluminescence for a neat 2CzPN film (60 nm, dashed line) is also reported for reference. Fig. 1b shows the chemical structure of the two molecules. DPEPO is a commonly used host material for blue emitters, featuring steric *ortho*-substituted diphenylphosphine oxide groups, which render the molecule highly polar.[31] On the other hand, 2CzPN is a thermally-activated delayed fluorescence emitter characterized by two electron-donating carbazolyl moieties attached to an electron-withdrawing dicyanobenzene ring with peak emission at 491 nm.[22] 2CzPN has been shown to lead to efficient blue light-emitting devices, including OLETs[32] and OLEDs.[33–35] 2CzPN exhibits its triplet energy level at around 2.5 eV,[36] smaller compared to that of DPEPO at 3.0 eV.[31] The relative position on the highest occupied molecular orbital (HOMO) and the lowest unoccupied molecular orbital (LUMO) of 2CzPN relative to DPEPO favours efficient charge transfer from the host to the guest, enabling efficient trapping of charge carriers on the emitter molecules and promoting radiative recombination from 2CzPN. Furthermore, a polar host can stabilize the charge-transfer (CT) excited state of the guest through local dipole interactions,[37] favouring a more efficient charge-transfer character of 2CzPN in the excited state.[38] We observed a redshift of the main emission peak with increasing 2CzPN concentration (with the largest shift occurring from 5 to 20%). Under our excitation conditions (λ_{exc} = 325 nm), DPEPO does not contribute to the emission (not shown). The time-resolved photoluminescence of the blends shows two decay times, indicating the TADF nature of 2CzPN, as shown in Fig. S1 (SI).

Aggregation,[39] intermolecular interactions,[40] and dipole–dipole interactions[41] have been shown to cause a redshift in the photoluminescence spectra. Aggregation, where molecules tend to self-assemble into larger structures ranging from small dimers and oligomers to extended clusters and solid-state formations, can lead to the formation of new excited states distinct from those of isolated molecules, thus altering the
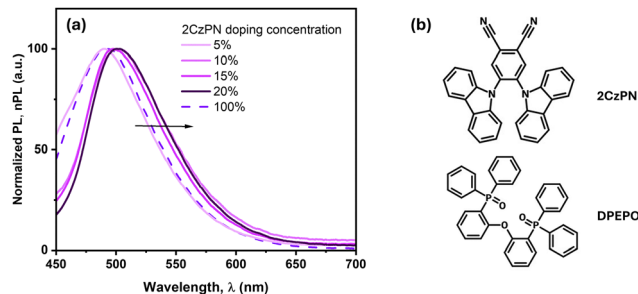

Fig. 1 (a) Normalized photoluminescence (nPL) spectra for DPEPO:2CzPN emissive blends deposited on quartz for different 2CzPN concentrations (as labelled). Photoluminescence of the 2CzPN neat film (dashed line) is also reported. (b) Chemical structure of 2CzPN (guest) and DPEPO (host).
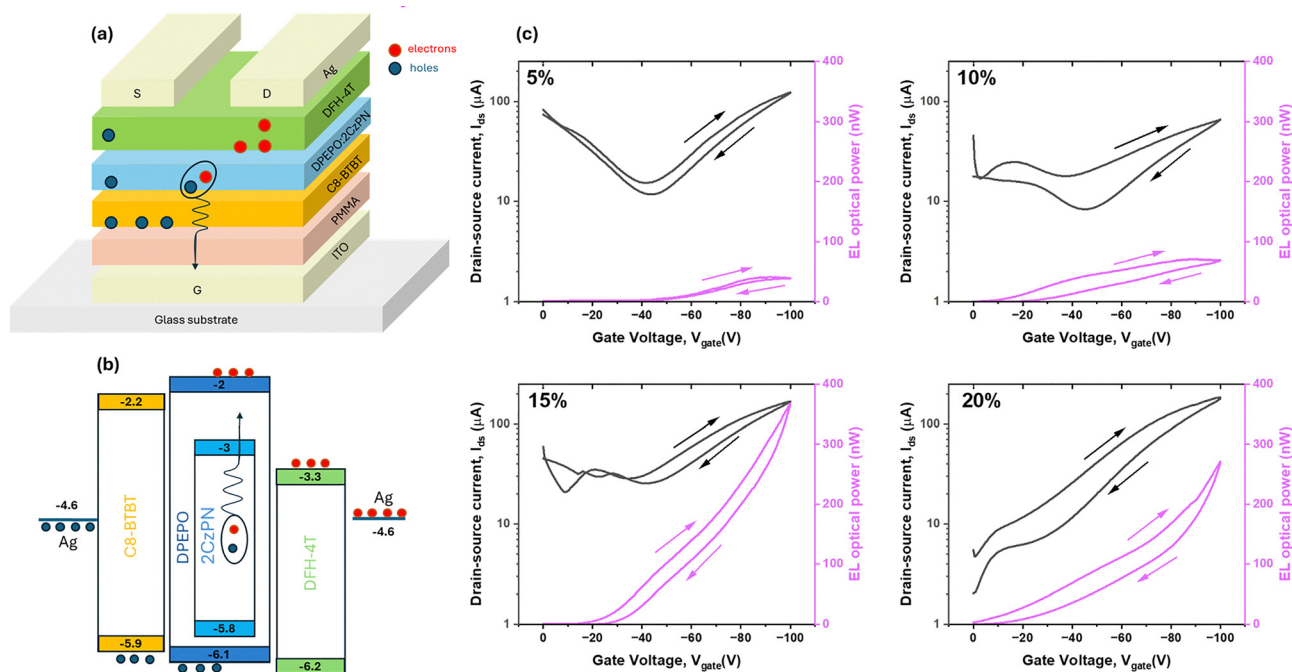
energy gap and shifting the main emission wavelength. Intermolecular interactions, including dipole–dipole forces, can also induce a different ground state formation than that of the isolated excited molecule.[40] Also, it has been shown that 2CzPN exhibits strong solvatochromism, leading to a redshift of its photoluminescence peak in more polar environments (host).[38]

3.2. Multilayer light-emitting field-effect transistor using DPEPO:2CzPN blends as the emissive layer

We fabricated bottom-gate top-contacts organic light-emitting transistors, as shown in Fig. 2a. The dielectric layer is a layer of PMMA (thickness of 400 nm), which was spin-coated and annealed under ambient conditions on top of the transparent ITO gate. PMMA has a smooth surface, offering a suitable dielectric/semiconductor interface.[42] The organic multilayer heterostructure includes three layers (3L): (from bottom to top) a C8-BTBT hole transport layer (30 nm) in direct contact with the dielectric layer, the DPEPO:2CzPN blend (60 nm) with different 2CzPN doping concentrations where charge carriers recombination and radiative decay occur, a DFH-4T electron transport layer (45 nm), and silver source and drain electrodes (70 nm). Materials and thickness for the semiconducting layers have been selected based on their high charge carrier mobilities;[12,43] for a more detailed characterization of the semiconducting layers, we refer the reader to some of our previous work.[44,45] Achieving higher performances in OLETs requires both balanced charge injection and efficient charge carrier transport.[16,46]

Fig. 2b shows the energy diagram of our multilayer organic stack. Favourable energy level alignment is crucial for facilitating efficient charge injection from the electrodes into the transport layers and subsequently from the transport layers towards the emissive layer. We refer the reader to the work in ref. 47 for general considerations on these materials and their energetics of the multilayer hetero-structures and materials therein. Fig. 2c shows the saturation transfer characteristics (I_{ds} *vs.* V_{gate} @V_{ds} = −100 V) of representative devices fabricated with emissive layers containing different 2CzPN content (as labelled). Light generated and extracted through the gate electrode (bottom emission) is also reported on the right *y*-

23030 | *J. Mater. Chem. C*, 2025, **13**, 23028–23036

This journal is © The Royal Society of Chemistry 2025

Fig. 2 (a) Simplified schematic of the multilayer transistor heterostructure and (b) its energy levels. (c) Saturation transfer curves (I_{ds} vs. V_{gate}@V_{ds} = −100 V) for **3L-OLET** with a DPEPO:2CzPN emissive layer with 2CzPN doping concentrations of 5, 10, 15, and 20%. The right y-axis refers to the electroluminescence light output (EL) measured through the gate electrode. Direction of sweeps is also indicated.

axis. We note here that measured light is only a fraction of the total light generated in the device. Both left- and right y-axes have the same scales in all four panels to favour a direct comparison. All the transistors have the same geometry, and all layers (semiconducting and electrodes) have been fabricated at the same time.

All organic light-emitting transistors exhibit ambipolar behaviour, with a relatively balanced charge transport (hole-dominated) for 2CzPN doping concentrations of 5, 10, and 15%. For higher 2CzPN doping concentration within the bend, the device tends to be less ambipolar, which is currently under investigation. In the saturation regime for an ambipolar transistor, the drain–source current can be described as:

$$I_{ds,sat} = \frac{W}{2L} C_i \left[\mu_{e,sat} \left(V_{gate} - V_{th,e} \right)^2 + \mu_{h,sat} \left(V_{ds} - \left(V_{gate} - V_{th,h} \right) \right)^2 \right] \quad (1)$$

where C_i is the capacitance per unit area of the dielectric layer (C_i (PMMA) = 6.6 nF cm^{-2}), μ_{sat} and V_{th} are the device saturation mobility and threshold voltages for holes (h) and electrons (e), and W (5 mm) and L (100 μm) are the transistor channel width and length, respectively. The field-effect saturation mobility and threshold voltage for both holes and electrons can be estimated from the linear fit of the forward sweep of the square root of I_{ds} vs. $V_{gate} = V_{ds}$ in the saturation region. In an ambipolar (multi-layer) transistor, light generation primarily occurs either (a) when charge transport is dominated by holes moving within the device, or (b) when both the hole and electron transport pathways are simultaneously active. In the vicinity of the curve apex, a more balanced charge density distribution leads to an increasing supply of minority charge carriers to the recombination area. We also observed hysteresis behaviour of the drain–source current in our devices, which we attributed to charge trapping in the channel.[48,49]

Table 1 summarizes the optoelectronic figures of merit for all the fabricated light-emitting transistors. Eight devices were

Table 1 Summary of the optoelectronic properties of organic light-emitting transistors with the emissive layer containing different 2CzPN doping concentrations

		2CzPN content (%)			
		5	10	15	20
Hole saturation mobility[a], μ_h	cm^2 V^{-1} s^{-1}	0.2	0.2	0.2	0.3
Hole threshold voltage[a], $V_{th,h}$	V	−34	−22	−34	−27
Electron saturation mobility[a], μ_e	cm^2 V^{-1} s^{-1}	0.1	0.03	0.03	0.002
Electron threshold voltage[a], $V_{th,e}$	V	39	24	24	24
External quantum efficiency, EQE@$V_{ds,max}$	%	0.01	0.065	0.058	0.03
ON/OFF ratio	× 10^5	2.7	88	47	7.3

[a] Forward sweep.

This journal is © The Royal Society of Chemistry 2025

J. Mater. Chem. C, 2025, **13**, 23028–23036 | **23031**

characterized for each emissive layer, leading to an approximate 5% uncertainty for the reported parameters. While hole mobility remains relatively independent of doping concentration, a significant decrease in electron mobility is observed with increasing 2CzPN doping concentration. We believe that this might be attributed to the reduction in the DPEPO content within the emissive layer; in fact, it is well known that DPEPO can efficiently transport electrons;[50] however, further studies are needed to elucidate this trend. Threshold voltages for holes were found to be in the range of -34 to -27 V, while those for electrons ranged from 24 to 39 V. These values are consistent with observations in organic light-emitting transistors using a low-k dielectric layer, such as PMMA.[51]

All devices exhibited negligible gate leakage currents, of the order of a few tens of nA within the applied bias range. Furthermore, the devices showed ON/OFF ratios of around 10^5, with no clear dependence on the doping concentration.

Fig. 3 shows the external quantum efficiency of our devices as a function of the 2CzPN doping concentration within the emissive blend; we found that a concentration of 2CzPN between 10% and 15% leads to improved device performances. This can be related to both electrical and optical properties of the used materials and their interfaces in the device architecture.[45]

The electrical properties of a material are strongly dependent on its molecular packing and the nature of its intermolecular interactions.[52] We studied the morphology of the various interfaces within the **3L-OLET** (Fig. S2, SI). We found a relatively smooth surface for C8-BTBT when deposited on PMMA, which affects the morphology of the emissive layer deposition, mimicking the C8-BTBT surface. No major differences in morphology and surface roughness as a function of the 2CzPN doping concentration are observed. On the other hand, although the topmost surface of the organic stack (DFH-4T layer) exhibits a very similar morphology across different

devices, the surface roughness shows a dependence on the doping of the emissive blend. These observations suggest that variations in the electrical properties within the device are not influenced by the PMMA/C8-BTBT or the C8-BTBT/EML interfaces,[52,53] while there is a contribution related to the surface roughness of the top DFH-4T layer within the device stack, which is consistent with previous studies.[54,55] In fact, the electron injection efficiency is governed not only by the energy barrier between the electrode Fermi level and the LUMO of the injection layer but also by the interfacial properties.[56] A rougher surface can potentially enhance the contact area between the electrode and the DFH-4T surface[57] and provide localized hotspots that can improve the charge injection efficiency.[56] Thus, the interplay between charge injection and transport influences the overall electrical performance in our light-emitting transistors.

Furthermore, the intrinsic optical properties of the blend can also affect the overall device efficiency.[58,59] In fact, by increasing the doping concentration, the number of emitting molecules naturally increases, which can lead to improved light generation. However, at high doping concentrations, Lee *et al.* have demonstrated that, unlike conventional fluorescent and phosphorescent molecules, the concentration quenching in TADF emitters is primarily governed by Dexter energy transfer, a process strongly dependent on intermolecular interactions.[60] In our case, as the doping concentration of 2CzPN increases, the intermolecular distances between adjacent 2CzPN molecules decrease exponentially, which favours Dexter energy transfer between the 2CzPN molecules, establishing non-radiative pathways.[59]

3.3. Optical and electrical excitation of the multilayer OLETs

For the rest of the discussion, based on a higher EQE, lower hole threshold voltage, and more balanced charge transport, we will focus our study on multilayer devices containing DPEPO:2CzPN 10%. Fig. 4a shows the normalized photoluminescence spectrum of such a blend on quartz (same data as in Fig. 1), and when integrated in two different multilayer heterostructure devices: **3L-OLET** (C8-BTBT/blend/DFH-4T as in Fig. 2a) and **2L-OLET** (C8-BTBT/blend). For the full optoelectronic characterization and analysis of our **2L-OLET** transistors with different 2CzPN content within the emissive layer, we refer the reader to the SI (Section (c): optoelectronic characterization of two-layer heterostructure OLETs (**2L-OLET**)). In the case of **3L-OLET**, we observed both a significant redshift (~ 15 nm) of the main emission peak along with its broadening as well as an additional spectral contribution at approximately 570 nm.

Photoluminescence spectra of the blend on quartz and in a 2L-stack are very similar to each other and do not exhibit this feature. For this, we have considered two possible mechanisms: exciton energy transfer[61] and exciplex formation.[62]

Exciton energy transfer[61] may occur when energy from an excited emissive layer is transferred to an adjacent layer (DFH-4T in our case), which can be followed by re-emission. In our case, the photoluminescence spectrum of the blend exhibits only minimal spectral overlap with the absorption spectra of DFH-4T (Fig. S5, SI), which rules out this mechanism.
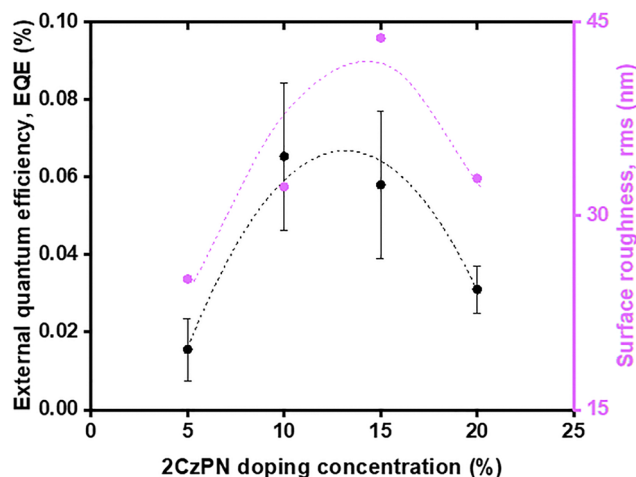

Fig. 3 (left y-axis) External quantum efficiency (at $V_{ds} = V_{gate} = -100$ V) and (right y-axis) surface roughness of the topmost deposited layer (DFH-4T) as a function of different 2CzPN doping concentrations within the emissive blend for **3L-OLET**. Dashed lines are a guide-to-the-eye only.
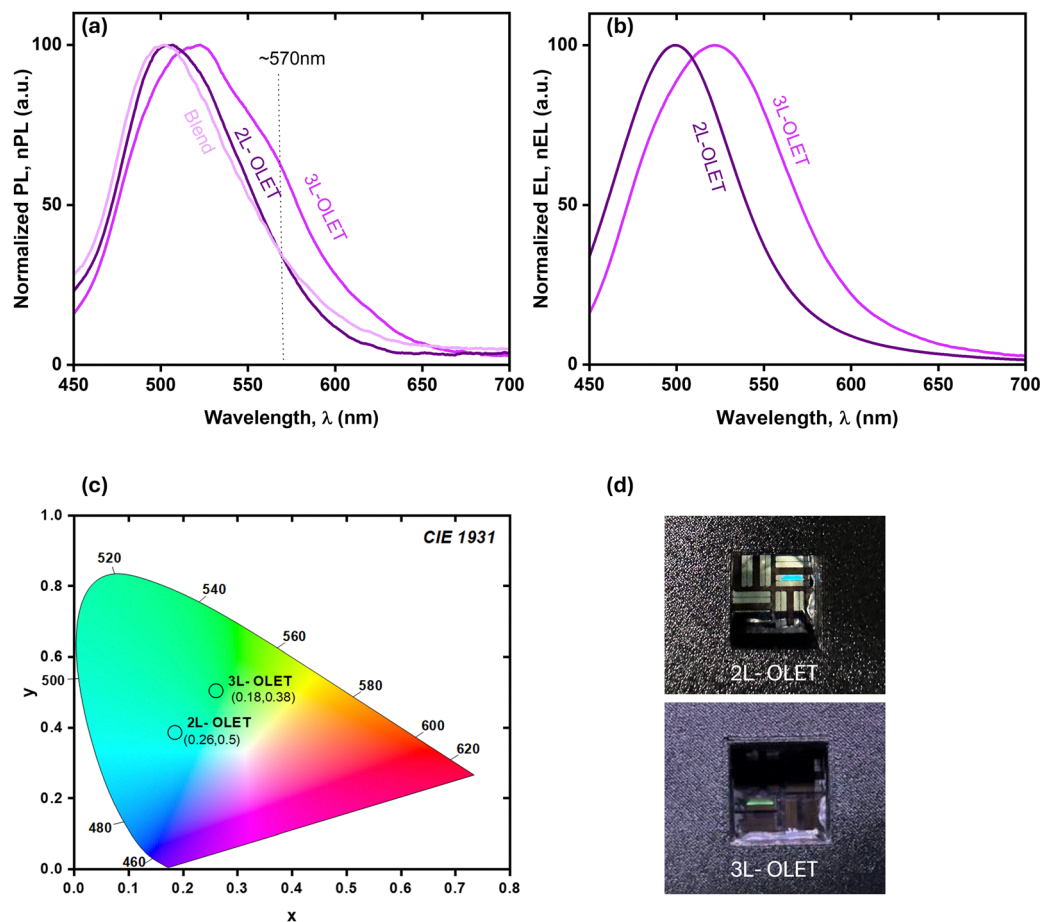
Fig. 4 (a) Normalized photoluminescence spectra of DPEPO:2CzPN 10 wt% on quartz and when integrated within the 2L- and 3L-device stacks. (b) Normalized electroluminescence spectra of 2L- and 3L-devices. (c) Colour coordinates (CIE 1931) and (d) optical images of **2L-OLET** and **3L-OLET**s in their ON-state (bottom emission, $V_{ds} = V_{gate} = -100$ V).

On the other hand, exciplexes, which are charge-transfer excitons, often result from molecular interactions between an electron donor and an electron acceptor molecule. Exciplexes can form either as bulk exciplexes through mixing donor and acceptor materials within a single layer or as interface exciplexes generated at the interface between distinct donor and acceptor layers. Previous studies have demonstrated that DPEPO and 2CzPN can independently lead to bulk exciplex in conjunction with different materials, provided the energy levels are appropriately matched.[63–67] These excitations, whether exciplex and/or excimers, occur within the bulk of the emissive layer, and, if any, they should exist in the active stack containing such emissive layer, regardless of the multilayer heterostructure considered (**3L-OLET** and **2L-OLET**). As for interface exciplexes, these are often associated with lower excitation quenching and enhanced radiative transition probability[68,69] and they are strongly dependent on the material energy level alignment and interfacial properties.

As shown in Fig. 2b, there is a significant energy barrier (~ 1.3 eV) for electron transport between the LUMOs of the DFH-4T layer and DPEPO layer, while a lower energy barrier (~ 0.2 eV) exists for hole transport from the HOMO of the C8-

BTBT layer to the HOMO of the DPEPO layer. This asymmetry in energy levels suggests that the electron transport from the DFH-4T layer into the emissive layer may be less efficient than that of hole transport from the C8-BTBT layer. Thus, this imbalance in charge transport can lead to an accumulation of electrons within the DFH-4T layer and an excess of holes at the interface between the DFH-4T and emissive layers. We believe that under these conditions, radiative recombination is favoured not only within the bulk of the emissive layer (originating from 2CzPN excitons) but also at such interface, resulting in the formation of interface exciplexes. The theoretically calculated binding energy of such interface exciplexes (2.5–2.8 eV), as determined by $E_{exciplex} = E_{LUMO,DFH-4T} - E_{HOMO, 2CzPN\ or\ DPEPO}$ shows good agreement with the observed additional contribution in the PL spectra of **3L-OLET** around 570 nm.[70]

Fig. 4b shows that, in the case of electrical excitation (EL), **3L-OLET** exhibits a distinct emission profile compared to **2L-OLET**, characterized by an overall red shift and broadened emission. Table 2 provides a summary of the spectral properties of the two-layer and three-layer devices. The full-width-half-maximum (FWHM) and emission wavelength of the 2L (EL) closely resemble the PL of the intrinsic blend and the 2L stack.

This journal is © The Royal Society of Chemistry 2025

J. Mater. Chem. C, 2025, **13**, 23028–23036 | **23033**

Table 2 Summary of luminescence characteristics of DPEPO:2CzPN 10% in different (device) configurations

	λ_{PL} (nm)	PL: FWHM (nm)	λ_{EL} (nm)	EL: FWHM (nm)
Blend on quartz	502	84	—	—
2L-OLET	505	84	499	81
3L-OLET	520	103	523	99

In contrast, the 3L device exhibits a broader FWHM and a redshift in its emission, which supports the contribution of exciplex formation to the overall emission. In the case of **2L-OLET,** we found a sky-blue emission with CIE 1931 coordinates of (0.26, 0.5), while for **3L-OLET** we observed a green emission, with CIE 1931 coordinates of (0.18, 0.38), as presented in Fig. 4c. Optical images of these organic light-emitting transistors in their ON-state are also shown in Fig. 4d. These strongly demonstrate the significant contribution of the DFH-4T layer and the resulting interface exciplex formation to the overall emission characteristics under electrical operation.

4. Conclusions

This work successfully demonstrated the integration of thermally-activated delayed fluorescence emitters within organic light-emitting transistors. We fabricated and investigated multilayer heterostructures incorporating 2CzPN, a blue-emitting TADF molecule, doped into the high-triplet-energy host DPEPO. Our findings confirmed that an approximate 10 wt% doping of 2CzPN in the DPEPO host yielded improved performance. We observed that two-layer devices (without an electron transport layer) exhibited light emission, characteristic of 2CzPN, whereas the addition of the electron transport layer led to both a redshift of the emission and the rise of an additional spectral contribution. This additional contribution is attributed to the formation of interfacial exciplexes at the emissive layer/electron transport interface.

Author contributions

A. A. conceived and carried out most of the experiments, analyzed the data, and wrote the manuscript. G. F. supported through additional experiments, AFM studies, data analysis, and validation. S. Y. and I. C. carried out the TRPL measurement and analysis. C. S. supervised the project. All authors contributed to the manuscript, provided feedback, and have given approval to its final version.

Conflicts of interest

There are no conflicts to declare.

Data availability

The data that support the findings of this study are available within the article and its supplementary information (SI) or available from the corresponding authors upon reasonable request. Supplementary information: (A) Time-resolved photoluminescence (TRPL) of DPEPO:2CzPN blends. (B) Morphology of different organic interfaces within the stack. (C) Optoelectronic characterization of two-layer heterostructure OLETs (**2L-OLET**). (D) Luminescence in organic heterostructures. See DOI: **https://doi.org/10.1039/d5tc02796a**.

Notes and references

1 S. R. Forrest, *Nature*, 2004, **428**, 911–918.
2 S. R. Forrest, *Organic electronics: foundations to applications*, Oxford University Press, USA, 2020.
3 M. C. Petty, *Organic and molecular electronics: from principles to practice*, John Wiley & Sons, 2019.
4 C. Zhang, P. Chen and W. Hu, *Small*, 2016, **12**, 1252–1294.
5 J. Liu, H. Zhang, H. Dong, L. Meng, L. Jiang, L. Jiang, Y. Wang, J. Yu, Y. Sun and W. Hu, *Nat. Commun.*, 2015, **6**, 10032.
6 G. Horowitz, *Adv. Mater.*, 1998, **10**, 365–377.
7 J. Song, H. Lee, E. G. Jeong, K. C. Choi and S. Yoo, *Adv. Mater.*, 2020, **32**, 1907539.
8 C. Rost, S. Karg, W. Riess, M. A. Loi, M. Murgia and M. Muccini, *Appl. Phys. Lett.*, 2004, **85**, 1613–1615.
9 J. Sobus, F. Bencheikh, M. Mamada, R. Wawrzinek, J. C. Ribierre, C. Adachi, S. C. Lo and E. B. Namdas, *Adv. Funct. Mater.*, 2018, **28**, 1800340.
10 H.-H. Hsieh, W.-C. Chen, G. Generali, C. Soldano, R. D'Alpaos, G. Turatti, V. Biondo, M. Muccini, E. Huitema and A. Facchetti, *SID Symp. Dig. Tech. Pap.*, 2016, **47**, 739–742.
11 M. Ullah, A. Armin, K. Tandy, S. D. Yambem, P. L. Burn, P. Meredith and E. B. Namdas, *Sci. Rep.*, 2015, **5**, 8818.
12 R. Capelli, S. Toffanin, G. Generali, H. Usta, A. Facchetti and M. Muccini, *Nat. Mater.*, 2010, **9**, 496–503.
13 M. U. Chaudhry, K. Muhieddine, R. Wawrzinek, J. Sobus, K. Tandy, S. C. Lo and E. B. Namdas, *Adv. Funct. Mater.*, 2020, **30**, 1905282.
14 H. Bronstein, C. B. Nielsen, B. C. Schroeder and I. McCulloch, *Nat. Rev. Chem.*, 2020, **4**, 66–77.
15 Y. Liu, C. Li, Z. Ren, S. Yan and M. R. Bryce, *Nat. Rev. Mater.*, 2018, **3**, 1–20.
16 C. Soldano, *Materials*, 2021, **14**, 3756.
17 M. Fahlman, S. Fabiano, V. Gueskine, D. Simon, M. Berggren and X. Crispin, *Nat. Rev. Mater.*, 2019, **4**, 627–650.
18 S.-Y. Cho, S.-Y. Kim, S. Jeon, R. Choi and J.-H. Lee, *Appl. Phys. Lett.*, 2019, **115**, 043301.

23034 | *J. Mater. Chem. C*, 2025, **13**, 23028–23036

This journal is © The Royal Society of Chemistry 2025

19 Z. Miao, C. Gao, M. Shen, P. Wang, H. Gao, J. Wei, J. Deng, D. Liu, Z. Qin and P. Wang, *Nat. Mater.*, 2025, **24**, 917–924.

20 V. Ahmad, J. Sobus, F. Bencheikh, M. Mamada, C. Adachi, S. C. Lo and E. B. Namdas, *Adv. Opt. Mater.*, 2020, **8**, 2000554.

21 Z. Pan, K. Liu, Z. Miao, A. Guo, W. Wen, G. Liu, Y. Liu, W. Shi, J. Kuang and Y. Bian, *Adv. Mater.*, 2023, **35**, 2209097.

22 H. Uoyama, K. Goushi, K. Shizu, H. Nomura and C. Adachi, *Nature*, 2012, **492**, 234–238.

23 S. Schmidbauer, A. Hohenleutner and B. König, *Adv. Mater.*, 2013, **25**, 2114–2129.

24 D. Volz, M. Wallesch, C. Fléchon, M. Danz, A. Verma, J. Navarro, D. Zink, S. Bräse and T. Baumann, *Green Chem.*, 2015, **17**, 1988–2011.

25 Y.-Z. Shi, H. Wu, K. Wang, J. Yu, X.-M. Ou and X.-H. Zhang, *Chem. Sci.*, 2022, **13**, 3625–3651.

26 H. Nakanotani, T. Higuchi, T. Furukawa, K. Masui, K. Morimoto, M. Numata, H. Tanaka, Y. Sagara, T. Yasuda and C. Adachi, *Nat. Commun.*, 2014, **5**, 4016.

27 H. Noda, H. Nakanotani and C. Adachi, *Sci. Adv.*, 2018, **4**, eaao6910.

28 D. Zhang, X. Song, M. Cai, H. Kaji and L. Duan, *Adv. Mater.*, 2018, **30**, 1705406.

29 G. Zhao, D. Liu, P. Wang, X. Huang, H. Chen, Y. Zhang, D. Zhang, W. Jiang, Y. Sun and L. Duan, *Angew. Chem.*, 2022, **134**, e202212861.

30 L. Song, Y. Hu, Z. Liu, Y. Lv, X. Guo and X. Liu, *ACS Appl. Mater. Interfaces*, 2017, **9**, 2711–2719.

31 Q. Zhang, T. Komino, S. Huang, S. Matsunami, K. Goushi and C. Adachi, *Adv. Funct. Mater.*, 2012, **22**, 2327–2336.

32 D.-K. Kim, Y.-L. Kim and J.-H. Choi, *J. Phys. Chem. C*, 2019, **123**, 11063–11072.

33 J. W. Sun, K.-H. Kim, C.-K. Moon, J.-H. Lee and J.-J. Kim, *ACS Appl. Mater. Interfaces*, 2016, **8**, 9806–9810.

34 M. Inoue, T. Serevičius, H. Nakanotani, K. Yoshida, T. Matsushima, S. Juršėnas and C. Adachi, *Chem. Phys. Lett.*, 2016, **644**, 62–67.

35 Y. Qi, J. Zhao, X. Wang, J. Yu and Z. Chi, *Org. Electron.*, 2016, **36**, 185–191.

36 Y. Olivier, B. Yurash, L. Muccioli, G. D'Avino, O. Mikhnenko, J.-C. Sancho-Garcia, C. Adachi, T.-Q. Nguyen and D. Beljonne, *Phys. Rev. Mater.*, 2017, **1**, 075602.

37 S. Melnykov, I. Helzhynskyy, T. Bulavinets and P. Stakhira, *East Eur. J. Phys.*, 2024, 31–42.

38 S. Kumar, P. Tourneur, J. R. Adsetts, M. Y. Wong, P. Rajamalli, D. Chen, R. Lazzaroni, P. Viville, D. B. Cordes and A. M. Slawin, *J. Mater. Chem. C*, 2022, **10**, 4646–4667.

39 E. Skuodis, O. Bezvikonnyi, A. Tomkeviciene, D. Volyniuk, V. Mimaite, A. Lazauskas, A. Bucinskas, R. Keruckiene, G. Sini and J. V. Grazulevicius, *Org. Electron.*, 2018, **63**, 29–40.

40 P. Filipek, K. Karoń, H. Hellwig, A. Szłapa-Kula and M. Filapek, *Materials*, 2022, **15**, 8525.

41 C. Han, Z. Zhang, D. Ding and H. Xu, *Chemistry*, 2018, **4**, 2154–2167.

42 K. Gallegos-Rosas, A. Azari and C. Soldano, *ACS Appl. Electron. Mater.*, 2025, **7**, 1274–1282.

43 K. Haase, C. Teixeira da Rocha, C. Hauenstein, Y. Zheng, M. Hambsch and S. C. Mannsfeld, *Adv. Electron. Mater.*, 2018, **4**, 1800076.

44 K. Gallegos-Rosas, P. Myllymäki, M. Saarniheimo, S. Sneck, R. Raju and C. Soldano, *ACS Appl. Electron. Mater.*, 2024, **6**, 1493–1503.

45 C. Soldano, O. Laouadi and K. Gallegos-Rosas, *ACS Omega*, 2022, **7**, 43719–43728.

46 Z. Qin, H. Gao, H. Dong and W. Hu, *Adv. Mater.*, 2021, **33**, 2007149.

47 C. Soldano, A. Stefani, V. Biondo, L. Basirico, G. Turatti, G. Generali, L. Ortolani, V. Morandi, G. P. Veronese and R. Rizzoli, *ACS Photonics*, 2014, **1**, 1082–1088.

48 R. Capelli, F. Dinelli, S. Toffanin, F. Todescato, M. Murgia, M. Muccini, A. Facchetti and T. J. Marks, *J. Phys. Chem. C*, 2008, **112**, 12993–12999.

49 M. Egginger, S. Bauer, R. Schwödiauer, H. Neugebauer and N. S. Sariciftci, *Monatsh. Chem.*, 2009, **140**, 735–750.

50 J. Zhang, D. Ding, Y. Wei and H. Xu, *Chem. Sci.*, 2016, **7**, 2870–2882.

51 C. Soldano, G. Generali, E. Cianci, G. Tallarida, M. Fanciulli and M. Muccini, *Thin Solid Films*, 2016, **616**, 408–414.

52 M. Kitamura and Y. Arakawa, *J. Phys.: Condens. Matter*, 2008, **20**, 184011.

53 M. Geiger, R. Acharya, E. Reutter, T. Ferschke, U. Zschieschang, J. Weis, J. Pflaum, H. Klauk and R. T. Weitz, *Adv. Mater. Interfaces*, 2020, **7**, 1902145.

54 K. Gallegos-Rosas, A. Azari and C. Soldano, *ACS Appl. Electron. Mater.*, 2025, **7**(3), 1274–1282.

55 J.-F. Chang, W.-R. Chen, S.-M. Huang, Y.-C. Lai, X.-Y. Lai, Y.-W. Yang and C.-H. Wang, *Org. Electron.*, 2015, **27**, 84–91.

56 Z.-H. Lu, J.-X. Hu, Y.-N. Zhong, X. Zhou, C. Xu, X. Gao, J.-L. Xu, S. Duhm and S.-D. Wang, *Appl. Phys. Lett.*, 2018, **113**(4), 043302.

57 S. Moschetto, E. Benvenuti, H. Usta, R. Ozdemir, A. Facchetti, M. Muccini, M. Prosa and S. Toffanin, *Adv. Mater. Interfaces*, 2022, **9**, 2101926.

58 H. Tang, X. Wang, Y. Li, W. Wang and R. Sun, *Displays*, 2008, **29**, 502–505.

59 H. S. Kim, S.-R. Park and M. C. Suh, *J. Phys. Chem. C*, 2017, **121**, 13986–13997.

60 J. Lee, N. Aizawa, M. Numata, C. Adachi and T. Yasuda, *Adv. Mater.*, 2016, **29**(4), 1604856.

61 F. Laquai, Y. S. Park, J. J. Kim and T. Basché, *Macromol. Rapid Commun.*, 2009, **30**, 1203–1231.

62 M. Sarma and K.-T. Wong, *ACS Appl. Mater. Interfaces*, 2018, **10**, 19279–19304.

63 T.-L. Wu, S.-Y. Liao, P.-Y. Huang, Z.-S. Hong, M.-P. Huang, C.-C. Lin, M.-J. Cheng and C.-H. Cheng, *ACS Appl. Mater. Interfaces*, 2019, **11**, 19294–19300.

64 H. J. Jang and J. Y. Lee, *Org. Electron.*, 2019, **75**, 105441.

65 H. J. Jang and J. Y. Lee, *J. Phys. Chem. C*, 2019, **123**, 26856–26861.

This journal is © The Royal Society of Chemistry 2025

J. Mater. Chem. C, 2025, **13**, 23028–23036 | **23035**

66 M. Zhang, C.-J. Zheng, H. Lin and S.-L. Tao, *Mater. Horiz.*, 2021, **8**, 401–425.

67 N. Nishimura, Z. Lin, K. Jinnai, R. Kabe and C. Adachi, *Adv. Funct. Mater.*, 2020, **30**, 2000795.

68 O. P. Dimitriev, *Chem. Rev.*, 2022, **122**, 8487–8593.

69 J. Gu, Z. Tang, H. Guo, Y. Chen, J. Xiao, Z. Chen and L. Xiao, *J. Mater. Chem. C*, 2022, **10**, 4521–4532.

70 X. K. Liu, Z. Chen, C. J. Zheng, C. L. Liu, C. S. Lee, F. Li, X. M. Ou and X. H. Zhang, *Adv. Mater.*, 2015, **27**, 2378–2383.

23036 | *J. Mater. Chem. C*, 2025, **13**, 23028–23036

This journal is © The Royal Society of Chemistry 2025